

Charge transport through a semiconductor quantum dot-ring nanostructure

Marcin Kurpas¹, Barbara Kędzierska¹, Iwona Janus-Zygmunt¹, Anna Gorczyca-Goraj¹, Elżbieta Wach², Elżbieta Zipper¹ and Maciej M Maśka¹

¹Department of Theoretical Physics, University of Silesia, Uniwersytecka 4, 40-007 Katowice, Poland

²Faculty of Physics and Applied Computer Science, AGH University of Science and Technology, Mickiewicza 30, 30-059 Kraków, Poland

E-mail: maciej.maska@us.edu.pl

Abstract. Transport properties of a gated nanostructure depend crucially on the coupling of its states to the states of electrodes. In the case of a single quantum dot the coupling, for a given quantum state, is constant or can be slightly modified by additional gating. In this paper we consider a concentric dot–ring nanostructure (DRN) and show that its transport properties can be drastically modified due to the unique geometry. We calculate the dc current through a DRN in the Coulomb blockade regime and show that it can efficiently work as a single electron transistor or a current rectifier. In both cases the transport characteristics strongly depends on the details of the confinement potential. The calculations are carried out for low and high bias regime, the latter being especially interesting in the context of current rectification due to fast relaxation processes.

PACS numbers: 73.23.Hk, 73.21.La, 73.22.-f

1. Introduction

In order to meet growing demand for small scale, low-power consuming devices one has to downscale transistors and logic circuits and to work with a small number of carriers. The natural limit for lowering carrier density is single charge electronics, where phenomena such as electric current can be controlled with single electron precision [1, 2]. Contrary to modern mass production electronics, single and a few electron devices exhibit purely quantum mechanical effects such as resonant tunneling [1–5] or quantum entanglement [6–8]. Apart from direct applications in nanoelectronics they are also perfect tools for probing fundamental problems in single and many-body physics. During the last decade a lot of research has been devoted to study the electronic properties of quantum dots (QD) [5, 9–14]. For sufficiently low temperatures the discreteness of the energy spectrum of these systems can be clearly visible in transport experiments as Coulomb peaks [1, 4, 15, 16] that demonstrate successive charging and discharging of the QD by single electrons. The Coulomb blockade phenomenon, where the charging energy forbids an electron to jump to the QD, is the basis for most of the applications of QDs [17–19]. Quantum dots arranged into double, triple or more complex systems [20–28] exhibit abundance of quantum states which manifest themselves, e.g., in Pauli spin blockade [29, 30] current or heat rectification [13] effects.

Another class of interesting quantum systems are quantum rings (QR) [31–35]. Due to different from QDs geometry the phenomena observed in QRs are very sensitive to phase coherence of the electronic wave function. These are, e.g., the Aharonov-Bohm effect demonstrating modification of the electron wave function by a vector potential [36] or persistent currents, i.e., ground state currents that flow in QR even without an external magnetic field [37–39].

In this paper we focus on a complex nanostructure that combines the two mentioned above, topologically different components: a quantum dot and a quantum ring. The constituents are aligned concentrically (QD is surrounded by QR) so that the system conserves the circular symmetry. The dot-ring nanostructure (DRN) has already been fabricated by pulsed droplet epitaxy [40, 41] with full control of the growth process. It can also be made by using atomic force microscope to locally oxidize the surface of a sample [12] or by lithography. Another method would be to grow a core-shell nanowire [42, 43] of, e.g., (In,Ga)As, where the core and shell parts are separated by a tunneling barrier. Then by cutting a slice of it one can form a DRN. A DRN exhibits a large variety of quantum states [44] what leads to many interesting features.

It has been recently shown [45, 46] that many measurable properties of a DRN, like spin relaxation or optical absorption, can be widely changed by a modification of the confinement potential of the DRN demonstrating its very high controllability and flexibility. These characteristics are mostly determined by the relative distribution of the wave functions in a DRN that, in turn, can be changed by external gates or fields. The purpose of this study is to demonstrate that also conducting properties of a DRN are very sensitive to the details of confinement and that we can realize different single

electron devices on this complex structure. Unlike field effect transistors, single electron devices are based on intrinsically quantum phenomenon, namely the tunnel effect. In this case transport properties are mostly determined by the tunneling rates Γ 's, which depend on the overlap of the DRN states with the states of the electrodes. These parameters, in turn, depend crucially on the localization of the electron wave function: states localized in QD (QR) are weakly (strongly) coupled to the electrodes. Thus Γ 's may strongly depend on the quantum state and have to be determined for each state individually. This property demonstrates one of the advantages of the DRN over QDs, where the possible changes of the couplings are orders of magnitude smaller.

We discuss charge transport through a DRN in the Coulomb blockade regime near the $N = 0 \leftrightarrow 1$ transition, i.e., when only one electron at a time can tunnel through a DRN between the source (S) and drain (D) electrodes. Throughout this paper we assume the magnetic field $B = 0$ and therefore neglect the electron spin. We show that one can tune the device parameters so that it can work as: (i) single electron transistor [4, 47] and (ii) electrical current rectifier. The paper is organized as follows: In Sec. 2 we present a general theoretical background that will be needed to study the transport properties of DRNs. In Sec. 3 we demonstrate how by changing the parameters of the confinement potential we can control single electron tunneling and build a single electron transistor (SET). In Sec. 4 we demonstrate that a DRN can be used as a current rectifier. The results are summarized in Sec. 5.

2. Basic formulas and mechanisms

We consider a quasi-two-dimensional circularly symmetric dot-ring nanostructure. The DRN, placed in the xy plane, is defined by a specific confinement potential, that we will discuss below. We assume that the confinement in the z (growth) direction is much stronger than the lateral confinement and consequently, the xy -plane motion and the vertical one can be decoupled. Then, we can write the electron wave function as a product

$$\psi(\mathbf{r}) = \psi_{||}(\mathbf{r})\psi_z(z), \quad (1)$$

where the vector \mathbf{r} lies in the xy -plane. Additionally, we assume that the electron is always in the lowest energy state of a quantum well in z direction and that the potential of the well in z direction is infinite. With these assumptions $\psi_z(z)$ is given by

$$\psi_z(z) = \sqrt{\frac{2}{d}} \cos\left(\pi \frac{z}{d}\right), \quad (2)$$

where d is the height of the structure.

In order to discuss the in-plane confinement potential that forms the DRN we introduce the following notation $|\mathbf{r}| = |(x, y)| = r$. Then the DRN is defined by a potential $V(r)$ and occupied by a *single* electron. The DRN is composed of a QD surrounded by a QR and separated from the ring by a potential barrier $V_0(r)$. A cross

section and a top view of a DRN with explanation of symbols used throughout the text is presented in figure 1.

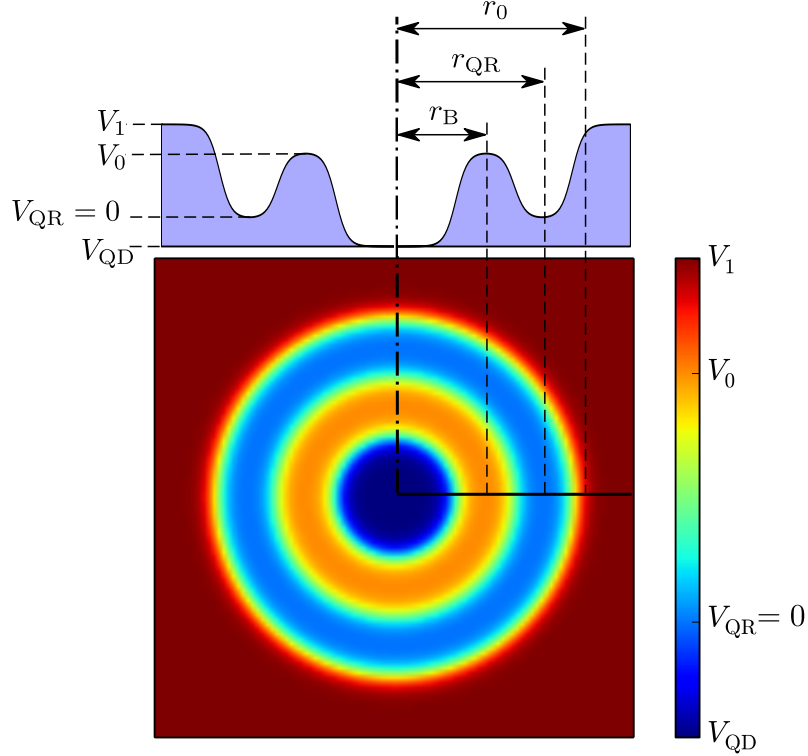


Figure 1. The cross section and the top view of the potential forming the DRN with marked bottom of the QD potential (V_{QD}), bottom of the QR potential (V_{QR}), top of the barrier potential (V_0) and the value of the potential outside the DRN (V_1). We assume the bottom of the quantum ring part as a reference value ($V_{QR} = 0$). This figure shows a DRN with the bottom of the QD below the bottom of the QR ($V_{QD} < 0$), but also the opposite situation ($V_{QD} > 0$) is possible.

In particular, we assume in our model calculations the radius of the DRN $r_0 = 70$ nm. The depth of the quantum well forming the DRN is $V_1 = 90$ meV and the zero potential energy is set at the level of V_{QR} , i.e., the potential well offset is equal V_{QD} . The calculations are performed for InGaAs systems (with the effective electron mass $m^* = 0.067m_e$). The results are presented for $V_0 = 20$ meV and for the sample thickness $d = 5$ nm, if not stated otherwise.

We solve numerically the Schrödinger equation assuming the Gaussian form of $V(r)$ [45]. The energy spectrum consists of a set of discrete states E_{nl} due to radial motion with radial quantum numbers $n = 0, 1, 2, \dots$, and rotational motion with angular momentum quantum numbers $l = 0, \pm 1, \pm 2, \dots$. The energy spectrum as a function of V_{QD} is shown in figure 2. The states situated in QD exhibit an increase of the energy with increasing V_{QD} , whereas those situated in QR have the energy (nearly) constant. The single particle wave function in the xy -plane, i.e., the DRN plane, is of the form

$$\psi_{||}(\mathbf{r}) \equiv \Psi_{nl}(r, \phi) = R_{nl}(r) \exp(il\phi), \quad (3)$$

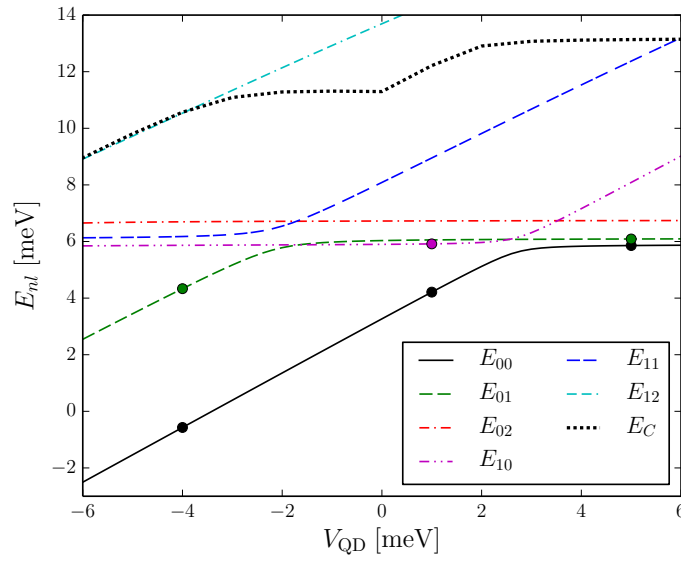


Figure 2. Energy spectrum of a DRN as a function of the position of the bottom of the QD potential V_{QD} . The circles indicate states for which wave functions are presented in figure 3. The dotted line shows the energy of the lowest two-electron state (see text in Sec. 3).

with the radial part $R_{nl}(r)$.

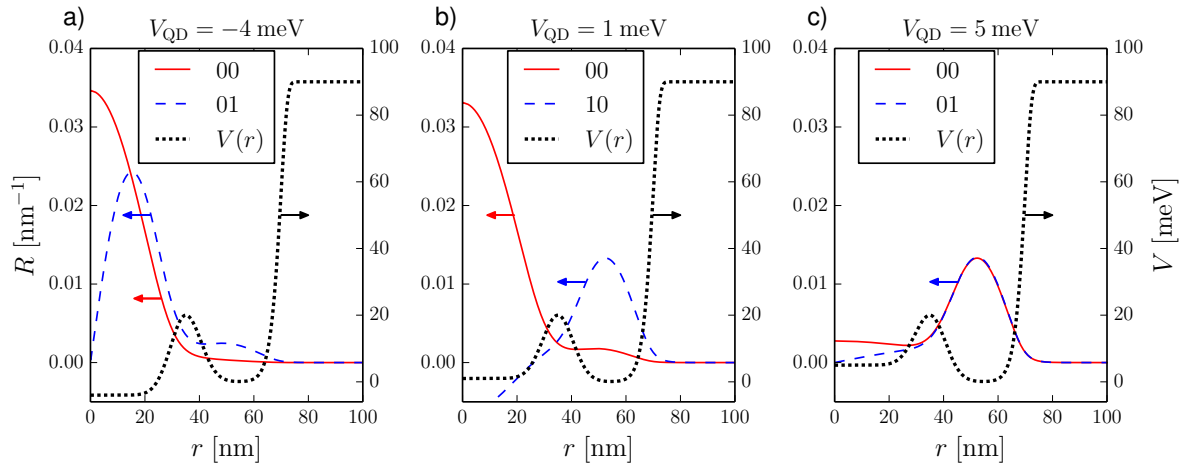


Figure 3. Radial parts of the wave functions of the two lowest states (red and blue lines) for different values of V_{QD} : -4 meV (a), 1 meV (b), and 5 meV (c). The black dotted line shows the corresponding shape of the confining potential $V(r)$

As already mentioned, the main advantage of the DRN is the controllability of the shape and the distribution of the electron wave functions. For instance, if the minimum of the potential of the QD part V_{QD} is much deeper than the potential of the QR, the

electrons are located mainly in the QD and the effective size of the ground state (G) wave function is small. On the other hand, if the ring's potential V_{QR} is much deeper electrons occupy mostly states in the QR part and the G wave function is much broader. What is more, by fine-tuning the confinement potential we can control positions of individual states. This way we are able to have, e.g., the ground state located in the QD, whereas the first excited state (E) in the QR and so on. The distributions of the wave functions of the two lowest energy states for three different values of V_{QD} are presented in figure 3. One can see there the case where both the G and E wave functions are in the QD for $V_{QD} = -4$ meV (figure 3a), the E wave function is in the QR, whereas the G wave function is still in the QD for $V_{QD} = 1$ meV (figure 3b), and finally, for $V_{QD} = 5$ meV both the G and E wave functions are in the QR (figure 3c).

The DRN is coupled via tunnel barriers to the S and D electrodes. We assume that one or a few (n_0) single-electron states are in the bias window

$$\mu_S > \epsilon_i > \mu_D, \quad i = 0, \dots, n_0 - 1, \quad (4)$$

where μ_S and μ_D are the respective chemical potentials, i represents a set of quantum numbers (n, l) and we start the numbering of the energy levels from $i = 0$ ($n = 0, l = 0$) (the ground state). Charge transport through a DRN depends crucially on the coupling strength of its states to the electrodes what is dependent on the wave function overlap that enters the electron tunneling matrix element. Because we are able to control the shape and distribution of the DRN wave functions, we can control the overlap, which, in turn, allows us to control the transport properties.

The tunneling rates Γ 's are calculated microscopically for each state independently. We follow Bardeen's approach [48], where

$$\Gamma(\epsilon) = 2\pi \sum_{\mathbf{k}} |t_{\mathbf{k}}|^2 \delta(\epsilon - \epsilon_{\mathbf{k}}). \quad (5)$$

Within the framework of this method two separate sets of states are considered: one solves the Schrödinger equation for the DRN and one for the electrode. It is implicitly assumed that the wave functions of the two subsystems are orthogonal. Enforcing this assumption the Bardeen tunneling matrix element in two dimensions is given by

$$t_{\mathbf{k}} = \frac{\hbar}{2m^*} \int_{-\infty}^{\infty} dy \left[\psi_{\mathbf{k}}^*(\mathbf{r}) \frac{\partial \Psi_{nl}(\mathbf{r})}{\partial x} - \Psi_{nl}(\mathbf{r}) \frac{\partial \psi_{\mathbf{k}}^*(\mathbf{r})}{\partial x} \right]_{x=x_0}, \quad (6)$$

where $\psi_{\mathbf{k}}(\mathbf{r})$ are wave functions in the electrode and $\Psi_{nl}(\mathbf{r})$ are wave functions in the DRN. The integral is calculated along the line $x = x_0$ (see figure 4). The explicit form of $t_{\mathbf{k}}$ is given in the Appendix.

2.1. Phonon relaxation in a DRN

When more than one state is included in the transport process one has to take into account mechanisms that allow transitions between the states, i.e., relaxation to the

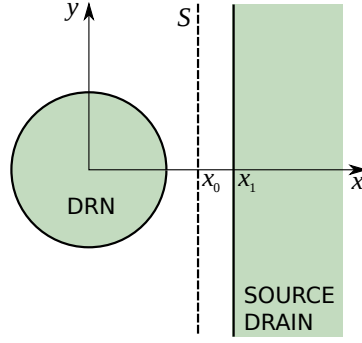


Figure 4. The geometry of the setup used to calculate the couplings Γ between the DRN and the electrodes.

lower energy states. One of the most important and unavoidable mechanisms of scattering in solid state systems is the interaction with lattice phonons. For low-dimensional semiconducting systems as QDs and QRs the dominant process is the electron-acoustic phonon interaction. This is because the energy distance between the electronic states is small comparing to the optical phonon energy [33, 49, 50].

In this section we calculate phonon emission relaxation rates due to interaction of an electron with piezoelectric (PZ) and deformational (DF) phonons. The electron-phonon scattering rate due to transition from the initial state $\psi^i(\mathbf{r})$ to the final state $\psi^f(\mathbf{r})$ with emission of an acoustic phonon can be calculated using Fermi's golden rule ($w_{i \rightarrow f} \equiv \tau_{i \rightarrow f}^{-1}$),

$$w_{i \rightarrow f} = \frac{2\pi}{\hbar} \sum_{\mathbf{q}, \lambda} |\langle \psi^f | \mathbf{W}_\lambda(\mathbf{q}) | \psi^i \rangle|^2 \delta(E_f - E_i - \hbar\omega_q), \quad (7)$$

where \mathbf{q} is the phonon wave vector, E_f (E_i) is the energy of the final (initial) electron state, $\hbar\omega_q$ is the energy of a phonon and λ is the polarization index. The interaction operator $\mathbf{W}_\lambda(\mathbf{q})$ is given by

$$\mathbf{W}_\lambda(\mathbf{q}) = \mathbf{A}_\lambda(\mathbf{q}) e^{-i\mathbf{q} \cdot \mathbf{r}}, \quad (8)$$

where $\mathbf{A}_\lambda(\mathbf{q})$ is the total scattering matrix element [33]

$$|\mathbf{A}_\lambda(\mathbf{q})|^2 = |\mathbf{A}_{\text{LA}}^{\text{DF}}|^2 + \sum_{\lambda=\text{LA, TA}} |\mathbf{A}_\lambda^{\text{PZ}}(\mathbf{q})|^2. \quad (9)$$

Because in this paper we focus mainly on transport properties of the DRN, we follow the reference [33] and use angular averaged piezoelectric coupling matrix element for longitudinal and transverse phonon modes. Thus, the total electron-phonon scattering matrix element can be written as [33, 51]

$$|\Lambda(\mathbf{q})|^2 = \frac{\hbar}{2\rho cV|\mathbf{q}|} (D^2|\mathbf{q}|^2 + P), \quad (10)$$

where D (P) is the deformational (piezoelectric) potential constant, ρ is the crystal density, c is the sound velocity, and V is the volume. After Refs. [33, 51] we assume

$D = 2.2 \times 10^{-18}$ J and $P = 5.4 \times 10^{-20}$ J²m⁻². The total relaxation rate from state $n'l'$ to state nl at $T = 0$ can be written as

$$w_{n'l' \rightarrow nl} = \frac{1}{4\pi^2 \hbar \rho c^2} q_0^3 (D^2 q_0^2 + P) \int_0^{2\pi} d\phi \int_0^{\pi/2} d\theta \sin \theta \times \left\{ \left| \int_0^\infty dr \int_0^{2\pi} d\phi' e^{i(l-l')\phi'} e^{iq_0 r \sin \theta \cos(\phi-\phi')} r R_{nl}(r) R_{n'l'}(r) \right|^2 \times \left| \frac{2}{d} \int_{-d/2}^{d/2} \cos^2 \left(\pi \frac{z}{d} \right) e^{-iz q_0 \cos \theta} dz \right|^2 \right\}, \quad (11)$$

where $q_0 = (E_{n'l'} - E_{nl})/\hbar c$ and $R_{nl}(r)$ is the radial part of the in-plane electron wave function $\psi_{||}(r)$. The integral over z is given by $f\left(\frac{1}{2}d q_0 \cos \theta\right)$, where

$$f(x) \equiv \frac{\pi^2}{\pi^2 x - x^3} \sin x \quad (12)$$

and the integral over ϕ' can be expressed by the Bessel function. Finally, the relaxation rate can be written as

$$w_{n'l' \rightarrow nl} = \frac{2\pi}{\hbar \rho c^2} q_0^3 (D^2 q_0^2 + P) \int_0^{\pi/2} d\theta \sin \theta F_{n'l',nl}^2(\theta), \quad (13)$$

where

$$F_{n'l',nl}(\theta) = f\left(\frac{1}{2}d q_0 \cos \theta\right) \int_0^\infty dr J_{|l-l'|}(q_0 r \sin \theta) r R_{nl}(r) R_{n'l'}(r). \quad (14)$$

Apart from material constants the factors that affect this rate are the energy gap between states $n'l'$ and nl , i.e., $E_{n'l'} - E_{nl}$, the mutual distribution of the wave functions given by $R_{nl}(r)$ and $R_{n'l'}(r)$, and the thickness of the structure d . Function $F_{n'l',nl}(\theta)$ describes how phonons emitted in different directions contribute to the relaxation process. The relaxation through phonons emitted at a given angle θ depends on d through function f given in equation (12). On the one hand, since its argument is $\frac{1}{2}d q_0 \cos \theta$ the relaxation is independent of the thickness d for phonons with wave vectors parallel to the xy plane ($\theta = \pi/2$). On the other hand, there is a strong dependence of the relaxation rate on d for phonons emitted in the direction perpendicular to nanostructure. Figure 5 shows $f^2(x)$. One can see there that for $\theta = 0$ a significant contribution to the relaxation comes only from phonons with wavelength larger than d .

Figure 6 shows the square of the function F given by equation (14) for $d = 5$ nm. The value of q_0 and the radial parts of the wave functions $R_{nl}(r)$ and $R_{n'l'}(r)$ have been calculated for two different values of V_{QD} . In the case presented in the left panel ($V_{\text{QD}} = -6$ meV) the bottom of the QD potential is much below the bottom of the QR potential. Therefore, the wave functions are situated mainly in the QD part of the DRN, where the energy level spacing is large (see figure 2). On the other hand, the right panel presents the case of $V_{\text{QD}} = 6$ meV where the bottom of the QD potential is above the bottom of the QR potential. In this situation the wave functions are situated mainly in the QR part of the DRN and, as it infers from figure 2, the level

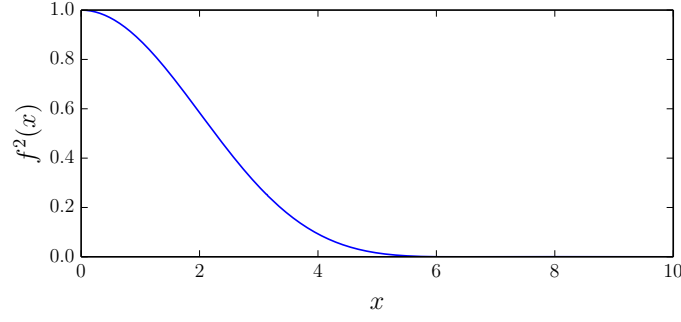


Figure 5. Square of the function $f(x)$ given by equation (12).

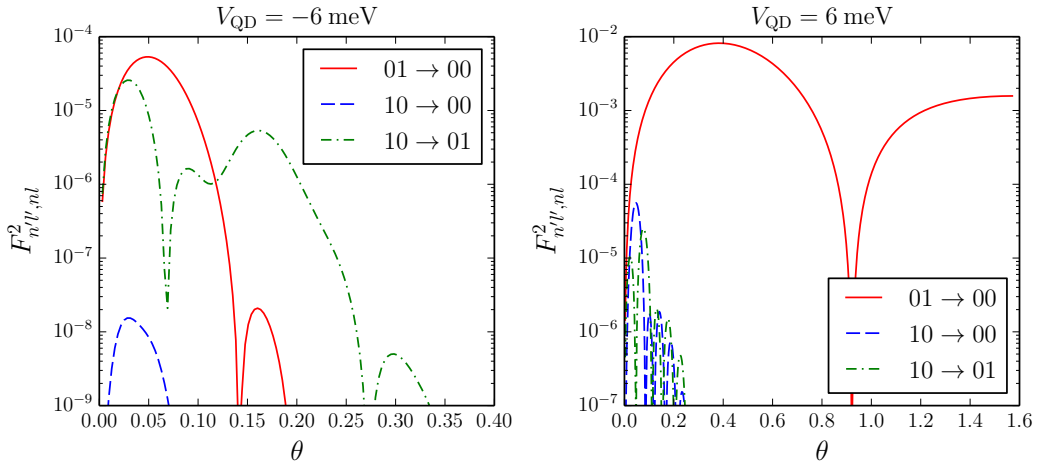


Figure 6. Square of the function $F_{n'l',nl}(\theta)$ given by equation (14) for two different values of V_{QD} for a DRN with $d = 5$ nm.

spacing is small. Figure 6 allows one to analyze the directions of phonons emission in two presented cases. Namely, in the left panel ($V_{\text{QD}} = -6$ meV) function $F_{n'l',nl}^2(\theta)$ describing the phonon emission is peaked within the range of low values of θ . This indicates that phonons are emitted mostly perpendicularly to the DRN, which is the direction of the strongest confinement [49]. In the complementary case presented in the right panel ($V_{\text{QD}} = 6$ meV), it is not possible to point out a specific direction of emission (it varies with a particular transition $n'l' \rightarrow nl$, note the difference in the scales on the horizontal axes).

Figure 7 shows typical examples of how the relaxation rates are affected by changing the position of the bottom of the QD potential V_{QD} from below to above the bottom of the QR potential ($V_{\text{QR}} = 0$). Figure 7a shows the relaxation rate from state ($n = 0, l = 1$) to the ground state ($n = 0, l = 0$). For large, negative value of V_{QD} both the wave functions Ψ_{00} and Ψ_{01} are positioned in the QD what gives fast relaxation with rates w of the order of GHz. With increasing V_{QD} the excited state

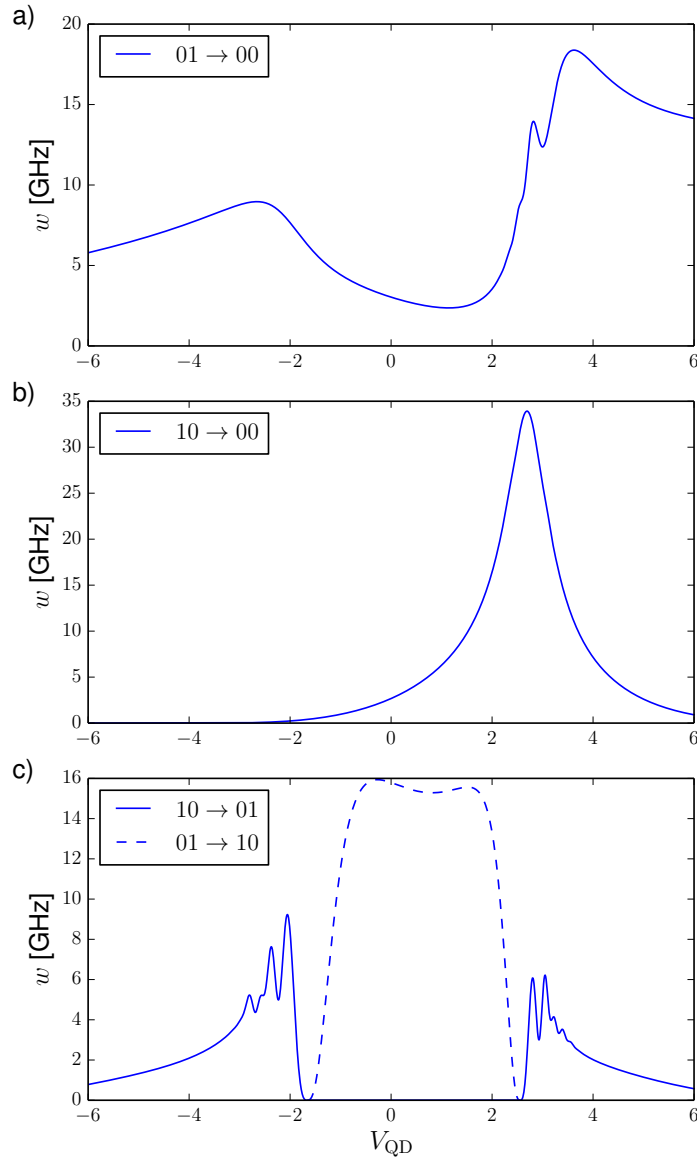


Figure 7. Illustrations of the dependence of different relaxation rates on V_{QD} for $d = 5$ nm. See the text for an explanation.

moves over to the QR leading to the decrease of the overlap between the wave functions what, in turn, results in the decrease of w . For further increased V_{QD} both the ground and the excited state are situated in the QR, the overlap increases and the relaxation rate increases again. Figure 7b presents the relaxation rate from state $(n = 1, l = 0)$ to the ground state. In this case for small V_{QD} the ground state is localized in the QD, while the excited state $(n = 1, l = 0)$ is mostly positioned in the QR. Therefore, the overlap of the corresponding wave functions is small, what in turn results in a slow relaxation. With the increase of V_{QD} the ground state starts to move over to the QR and the overlap with Ψ_{10} starts to rise. One observes it as a sharp increase of the relaxation

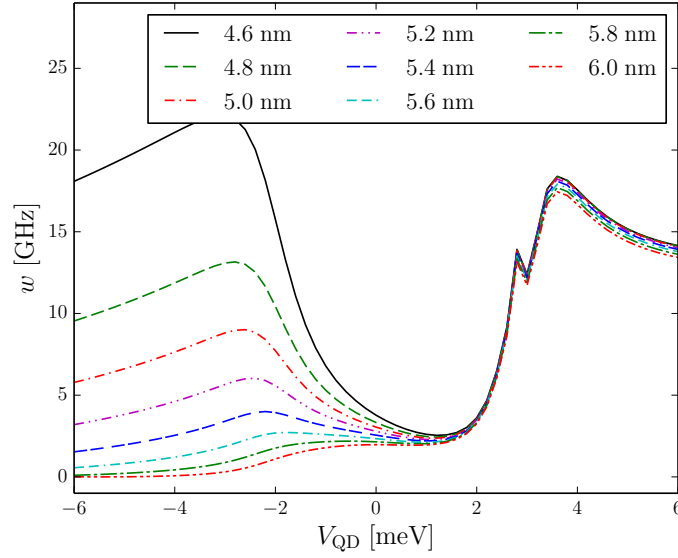


Figure 8. Relaxation rate $w_{01 \rightarrow 00}$ as a function of V_{QD} for different values of sample thickness.

rate $w_{10 \rightarrow 00}$. However, with further increase of V_{QD} the ground state remains in the QR, yet the excited state moves over to the QD and changes sign. This altogether causes the decrease of the relaxation rate. Figure 7c presents the relaxation rate between states $(n = 1, l = 0)$ and $(n = 0, l = 1)$, a transition that is a part of an indirect relaxation process. What is clearly visible at first glance is the abrupt decrease of $w_{10 \leftrightarrow 01}$ when the states cross (compare figure 2). In the range of V_{QD} from -2 meV to 2 meV the overlap between Ψ_{10} and Ψ_{01} is strong. Thus, the resulting values of the relaxation rate are high.

As it was already mentioned, the phonon emission at different angles is strongly dependent on the distribution of the wave functions (see figure 6). This, in turn affects the dependence of the relaxation rates on the sample thickness d . In figure 8 we present the relaxation rate $w_{01 \rightarrow 00}$ as a function of V_{QD} . Its dependence on d is pronounced for low values of V_{QD} , when the wave functions are situated mainly in the QD region of the DRN. In accordance with what was reported in Ref. [33] for QD's, we also observe oscillations of the relaxation rates as a function of the sample thickness d in the range of negative values of V_{QD} (yet in figure 8 we present only a part of the noted oscillations). In the range of low values of V_{QD} the level spacings are of the order of single meV's (figure 2). The corresponding wavelengths of emitted phonons are of the order of the sample thickness (couple of nm's). This match results in the strong increase of the relaxation rates for such V_{QD} . In the complementary range of V_{QD} , where the bottom of the QD potential is above the bottom of the QR potential, the level spacings are of order of 0.1 meV. Then, the corresponding wavelengths of emitted phonons are significantly larger than the sample thickness and we do not observe any strong dependence of $w_{01 \rightarrow 00}$ on the

thickness of the structure d . Additionally, we would like to stress the strong dependence of the relaxation rates for all other transitions $w_{n'l' \rightarrow nl}$ on d (not shown).

3. Single electron transistor

We are now ready to discuss the transport properties of the DRN. We evaluate the current given the energy spectrum and the subsequent relaxation and tunnel rates. We discuss below sequential tunneling current in the Coulomb blockade regime near the $N = 0 \leftrightarrow 1$ transition and neglect higher order tunneling events [52]. In the pure quantum dot case SET is switched to the conducting state when some energy level, shifted by gate voltage, enters the bias window. The current exhibits then the current peak [5]. In case of the DRN the mechanism is different. We keep one or a few states in the bias window and manipulate the distribution of the wave functions to get a proper transistor behavior. The principle of operations in is to control the energy states and tunnel couplings by means of gate voltages V_{QD} and V_0 . Many investigations of transport behavior make use of the high tunability of the tunnel barriers by applying voltage pulses [52]. In our approach we utilize instead the high tunability of the electron states in the DRN while keeping the barrier parameters constant. We assume that the bias window is smaller than the charging energy E_C , so that only a single electron at a time can be transmitted through the DRN, $|\mu_S - \mu_D| < E_C$. In order to determine for what values of the model parameters this condition can be fulfilled we calculate E_C for the DRN. The interaction energy of two particles confined in the potential $V(r)$ was calculated using the configuration interaction approach [53], which is an exact diagonalization method for solving the nonrelativistic Schrödinger equation for a multi-particle system. From the single-particle orbitals Ψ_{nl} we constructed the basis of the Slater determinants $|S_\mu\rangle$. Then, the two-particle Hamiltonian was diagonalized and the exact eigenstates were found where the ν -th eigenfunction is in the form of the linear combination of the Slater determinants:

$$\Phi_\nu = \sum_\mu c_{\mu\nu} |S_\mu\rangle. \quad (15)$$

Coefficients $c_{\mu\nu}$ were calculated by the two-particle Hamiltonian diagonalization. In figure 2 the energy E_C of the lowest two-particle state is shown by the black dotted line as a function of V_{QD} . It can be seen there that for the analyzed range of V_{QD} , E_C is larger than the five lowest single-particle levels.

The current through the DRN is calculated with the help of the rate equations. Assuming that n_0 energy levels lie in the bias window $\mu_S - \mu_D$, the time evolution of the occupation probability ρ_j of a given DRN state j can be expressed by the following formula:

$$\dot{\rho}_j = \Gamma_j^S \left(1 - \sum_{i=0}^{n_0-1} d_i \rho_i \right) + \sum_{i=j+1}^{n_0-1} d_i w_{i \rightarrow j} \rho_i - \left(\Gamma_j^D + \sum_{i=0}^{j-1} d_i w_{j \rightarrow i} \right) \rho_j. \quad (16)$$

Indices i and j denote pairs of quantum numbers (n, l) with $i = 0$ describing the ground

state ($n = 0; l = 0$); the states are ordered so that $\epsilon_i > \epsilon_j$ if $i > j$ and

$$d_i = \begin{cases} 1 & \text{if } i \text{ denotes a state with } l = 0, \\ 2 & \text{if } i \text{ denotes a state with } l > 0 \end{cases} \quad (17)$$

is the orbital degeneracy of i -th state ($E_{nl} = E_{n,-l}$). The processes that enter equation

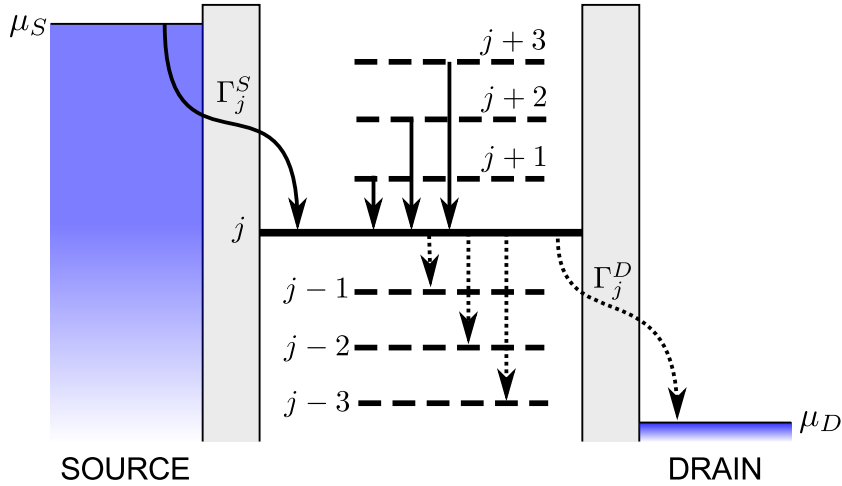


Figure 9. Processes included in equation 16. The solid (dotted) S-shape line represents the transfer of an electron from the source electrode to state j (from state j to the drain electrode). The vertical solid (dotted) lines represent relaxation from states above state j to state j (from state j to states below state j).

(16) are illustrated in figure 9. The first term on the r.h.s. describes the rate at which electrons tunnel from the S electrode. Due to the Coulomb blockade such a transfer is possible only when none of the DRN states is already occupied, what is ensured by the expression in parentheses. The second term describes relaxation to state j from higher-lying states. The last term describes tunneling to the D electrode and relaxations from state j to lower-lying states. If $j = n_0$ ($j = 0$) the second (third) sum in equation (16) should be omitted since there are no states from (to) which relaxation is possible.

As we are interested in the steady-state current we put $\dot{\rho}_j = 0$ in equation (16).

Then, introducing $\bar{\rho}_i \equiv d_i \rho_i$, the system of equations for ρ_j can be rewritten as

$$\begin{pmatrix} \Gamma_0^S + \frac{1}{d_0} \Gamma_0^D & \Gamma_0^S - w_{1 \rightarrow 0} & \Gamma_0^S - w_{2 \rightarrow 0} & \dots \\ \Gamma_1^S & \Gamma_1^S + \frac{1}{d_1} (\Gamma_1^D + w_{1 \rightarrow 0}) & \Gamma_1^S - w_{2 \rightarrow 1} & \dots \\ \Gamma_2^S & \Gamma_2^S & \Gamma_2^S + \frac{1}{d_2} (\Gamma_2^D + w_{2 \rightarrow 0} + w_{2 \rightarrow 1}) & \dots \\ \Gamma_3^S & \Gamma_3^S & \Gamma_3^S & \dots \\ \dots & \dots & \dots & \dots \\ \Gamma_{n_0-1}^S & \Gamma_{n_0-1}^S & \Gamma_{n_0-1}^S & \dots \end{pmatrix} \begin{pmatrix} \dots & \Gamma_0^S - w_{(n_0-1) \rightarrow 0} \\ \dots & \Gamma_1^S - w_{(n_0-1) \rightarrow 0} \\ \dots & \Gamma_2^S - w_{(n_0-1) \rightarrow 0} \\ \dots & \Gamma_3^S - w_{(n_0-1) \rightarrow 0} \\ \dots & \dots \\ \dots & \Gamma_{n_0-1}^S + \frac{1}{d_{n_0-1}} \left(\Gamma_{n_0-1}^D + \sum_{i=0}^{n_0-2} w_{(n_0-1) \rightarrow i} \right) \end{pmatrix} \begin{pmatrix} \bar{\rho}_0 \\ \bar{\rho}_1 \\ \bar{\rho}_2 \\ \bar{\rho}_3 \\ \dots \\ \bar{\rho}_{n_0-1} \end{pmatrix} = \begin{pmatrix} \Gamma_0^S \\ \Gamma_1^S \\ \Gamma_2^S \\ \Gamma_3^S \\ \dots \\ \Gamma_{n_0-1}^S \end{pmatrix} \quad (18)$$

In the absence of magnetic field d_0 is always equal to 1, but we have left it in the first row for consistency of notation.

The solutions can be easily found in limiting cases of a very slow relaxation and of a very weak couplings to the electrodes. In the former case, when we put $w_{i \rightarrow j} \rightarrow 0$ for all i and j , the solution for a symmetric coupling ($\Gamma_i^S = \Gamma_i^D$) takes on a simple form $\rho_i = 1/(n_0 + 1)$. In the latter case, when we put $\Gamma_i^S, \Gamma_i^D \rightarrow 0$ for all i , we get $\rho_i = 0$ for all $i > 0$, what means that only the ground state participates in the transport. In a general case the system of linear equations (18) can be solved analytically, but with increasing n_0 the formulas quickly become very long. With the help of the occupation probabilities ρ_i , the steady-state current can be expressed as a sum of currents I_i^{in} carried by electrons which tunnel from the S electrode to all the states that lie in the bias window. Since in the steady state the currents through both the barriers are equal, the total current can be also expressed as a sum of currents I_i^{out} carried by electrons which tunnel from the DRN to the D electrode. Then, the total current can be written as

$$I = \sum_{i=0}^{n_0-1} I_i^{\text{in}} = \sum_{i=0}^{n_0-1} I_i^{\text{out}}, \quad (19)$$

where the currents carried by electrons tunneling to and from individual levels are given by

$$I_i^{\text{in}} = e \Gamma_i^S (1 - \rho_i), \quad I_i^{\text{out}} = e \Gamma_i^D \rho_i. \quad (20)$$

We assume, following the experiments in Refs. [9, 10], $k_B T \approx 0.01$ meV. Thus, in our studies both the energy spacings and the bias window are much larger than the thermal energy and we neglect the temperature smearing out of the energy levels. Then

for a forward bias ($\mu_S - \mu_D > 0$) the electrons can tunnel only from the S electrode to the DRN and then from the DRN to the D electrode. The tunnel rates in equation (18) depend on the DRN geometry. We assume it so that Γ for the most strongly coupled state is equal to 5 GHz and calculate all the other couplings accordingly. That way all the tunnel rates are in the range of the experimentally accessible values [54].

We start with the low bias regime where only the ground state lies in the bias window ($n_0 = 1$). In this case the total current is given by equation (20) with the requirement that $I_0^{\text{in}} = I_0^{\text{out}}$:

$$I = e \frac{\Gamma_G^S \Gamma_G^D}{\Gamma_G^S + \Gamma_G^D}. \quad (21)$$

We assume symmetric tunneling barriers to the S and D electrodes $\Gamma_i^S = \Gamma_i^D$ and numerically calculate their values. The mechanism of the SET is as follows: if the bottom of the QD potential is significantly below the bottom of the QR potential, the ground state is localized in the QD near the center of the DRN. Since for a deep enough QD potential the wave function decreases almost exponentially with increasing distance from the QD, its overlap with the electrode's wave functions is negligible. With an increase of V_{QD} this state moves to the outer (QR) part of the structure where it has much larger overlap with the states in the electrodes. This results in a strong increase of the current. We calculate the current as a function of the gate voltage V_{QD} for three different values of V_0 . Results are presented in figure 10. One can see in this figure that

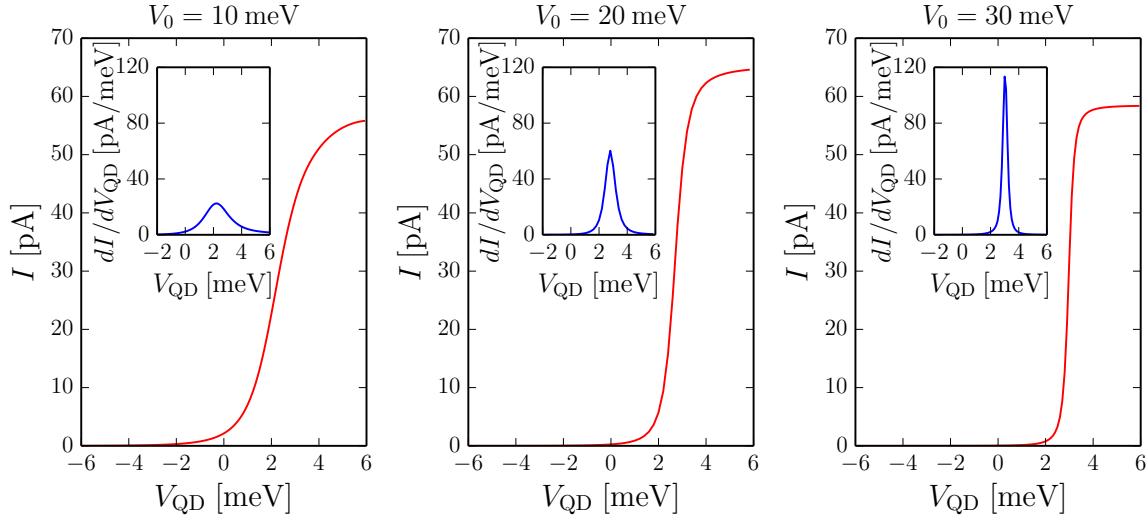


Figure 10. The current as a function of V_{QD} for three values of V_0 : 10, 20 and 30 meV. $\Gamma = 500$ MHz has been assumed in all the cases.

the steepness of the $I(V_{\text{QD}})$ characteristics increases significantly with an increase of V_0 . If V_0 is small, the ground state wave function gradually moves with increasing V_{QD} towards the outer part of the DRN. This leads to a slow increase of the current. On the other hand, if V_0 is large, there are two pronounced minima of the confining potential

(one in the QD and one in the QR) and with increasing V_{QD} at some point the ground state wave function “jumps” from the QD to the QR. It results in a step-like $I(V_{\text{QD}})$ characteristics. This dependence is clearly seen in the insets in figure 10, where the differential conductance dI/dV_{QD} is presented for different heights of the barrier V_0 separating the DRN.

The low bias limit, however, not always can be reached. In many cases the evolution of the DRN’s spectrum shows several level crossings when V_{QD} is changed. In such cases the bias $\mu_S - \mu_D$ cannot be adjusted to include only the ground state for all values of V_{QD} for which the transistor effect occurs. We see in figure 2 that depending on V_{QD} two or three (or even more) states have to be accounted for. It is known that transport in the Coulomb blockade regime can be suppressed by the occupation of excited states [55]. Therefore, we analyze below how the system should be designed to get a good transistor behavior in the high bias regime. The dc currents are calculated as steady state solutions to the rate equations [equations (18-20)] for the occupation probabilities for all relevant states considering all the processes transferring electrons, namely the tunnel rates Γ ’s and subsequent relaxation rates w ’s. It turns out that the major factor that determines the current is the relations between the tunnel and relaxation rates. When the coupling to the electrodes is small compared to the corresponding relaxation rates, most of electrons that travel through the DRN will relax to the ground state before leaving the DRN by tunneling to the drain electrode. Then, the total current is determined mostly by the transport only through the ground state even if some of the excited states are in the bias window. In this case the system behaves like in the described above low bias limit. This situation is illustrated in figure 11.

What we have also noted from our numerical calculations is that if the relaxation rates w ’s are comparable to the coupling constants Γ ’s, then only a minor influence of higher excited states appears. They do not change the switching characteristics but increase the current amplitude.

As follows from the calculations in Sec. 2.1 the relaxation rates are of the order of a few GHz in the broad range of V_{QD} . Therefore, one can easily obtain Γ ’s smaller or comparable to the corresponding relaxation rates and consequently get the desired transistor behavior, as shown in the inset in figure 11b.

4. Current rectifier

Current rectification plays an important role in electron transport and is fundamental for the development of novel basic elements in nanoelectronics. The attempts have been made to build downscaled rectifiers. Coulomb blockade rectifier on a triple dot system [26, 56] has been recently introduced. Rectification properties of a quantum wire coupled asymmetrically to a quantum dot have also been studied [57]. We propose here a rectifier built on a DRN which utilizes different distribution of the ground and excited states wave functions.

To show the idea we discuss at first a case where the two lowest states are in the

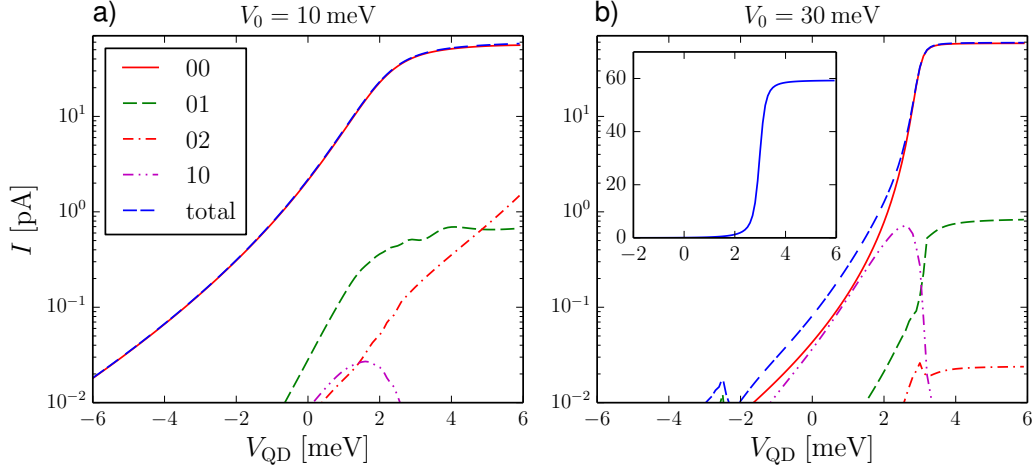


Figure 11. The total current along with contributions that flow through particular DRN's levels for $\Gamma = 500$ MHz, $V_0 = 10$ meV (a) and $V_0 = 30$ meV (b). In both panels the meaning of the lines is the same. The inset in the right panel shows the total current in non-logarithmic scale.

bias window and we present the analytical solutions for the currents.

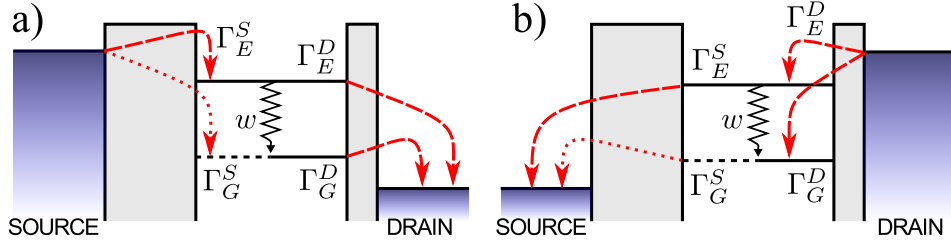


Figure 12. The scheme of a rectifier with two energy levels in the bias window for forward (a) and reverse (b) bias. The red dotted line represents the tunneling rate Γ_G^S between the source electrode and the ground state that is assumed to be extremely small. The solid zig-zag line represent the relaxation w from the excited state.

The confinement potential of the DRN is tuned so that the first excited state (E) has significantly larger overlap with the leads than the ground state (G). Thus, the same holds true for the corresponding tunneling rates, i.e., $\Gamma_G \ll \Gamma_E$. To get current rectification we have to break the left-right symmetry, therefore we assume an asymmetric coupling to the source and drain electrodes, i.e., the drain electrode is much closer to the DRN than the source one. This results in the following relations between the tunneling rates:

$$\Gamma_i^S \ll \Gamma_i^D \quad (i = G, E), \quad (22)$$

where Γ_G^S is assumed to be so small that the current between the ground state and the source electrode is negligible ($\Gamma_G^S \leq 100$ kHz [5]). One can tune the distances between the DRN and electrodes to ensure the above relation. Moreover, it follows from equations

in the Appendix that the ratio of the tunneling rates to the ground and excited states is independent of this distance, so that

$$\frac{\Gamma_G^S}{\Gamma_E^S} = \frac{\Gamma_G^D}{\Gamma_E^D}, \quad (23)$$

what is on line with the assumptions made, e.g., in Refs. [10, 54] in the interpretation of their experiments.

The proposed mechanism of the rectification is the following: for forward bias ($\mu_S - \mu_D > 0$, see figure 12a) the current from the source electrode flows to the DRN through the excited state and then either further flows to the drain electrode through the excited state or the electron relaxes and leaves the DRN through the ground state. This is the forward direction of the rectifier. On the other hand, for reverse bias ($\mu_S - \mu_D < 0$, see figure 12b) an electron can enter either the ground or the excited state. If the electron enters the ground state, it cannot leave the DRN because of the negligible coupling to the source electrode (we assume the temperature to be low enough to prevent from exciting the electron to the next energy level and from tunneling back to the drain electrode). If the electron enters the excited state, it will relax to the ground state due to fast relaxation (Sec. 2). Then, in either case the electron gets stuck in the ground state blocking the current through the excited state by means of the Coulomb blockade. This is the reverse direction of the rectifier.

To describe the proposed rectifier effect in a quantitative way we calculate the currents using the steady state solutions of the rate equations for the occupation probabilities [equations (18-20)]. Taking into account only the two lowest states we obtain the current I_F for the forward bias and the reverse current I_R for the reverse bias:

$$I_F = e\Gamma_E^S \frac{d_1 (\Gamma_E^D + w)}{\Gamma_E^D + d_1 w \left(1 + \frac{\Gamma_E^S}{\Gamma_G^D}\right)}, \quad (24)$$

$$I_R = -e\Gamma_G^S \frac{w + \Gamma_E^S}{w}, \quad (25)$$

where w is the relaxation rate for the first excited state and d_1 is its degeneracy. These formulas allow us to find the conditions under which DRN behaves as a rectifier, i.e., for which

$$\left| \frac{I_F}{I_R} \right| \gg 1. \quad (26)$$

Since $\Gamma_E^S \ll w$ we get

$$\left| \frac{I_F}{I_R} \right| = \frac{\Gamma_E^S}{\Gamma_G^S} \frac{d_1 (\Gamma_E^D + w)}{\Gamma_E^D + d_1 w \left(1 + \frac{\Gamma_E^S}{\Gamma_G^D}\right)}. \quad (27)$$

One can see that the ratio of the forward and reverse currents depends crucially on the ratio between couplings of the ground and excited states to the S electrode and this is a parameter that can easily be tuned in a DRN.

We calculate the tunneling rates Γ_E^S , Γ_G^S and Γ_E^D , Γ_G^D and the relaxation rates w as a function of V_{QD} under the assumption that the geometry of the DRN is that the maximal value of Γ_E^D is 5 GHz.

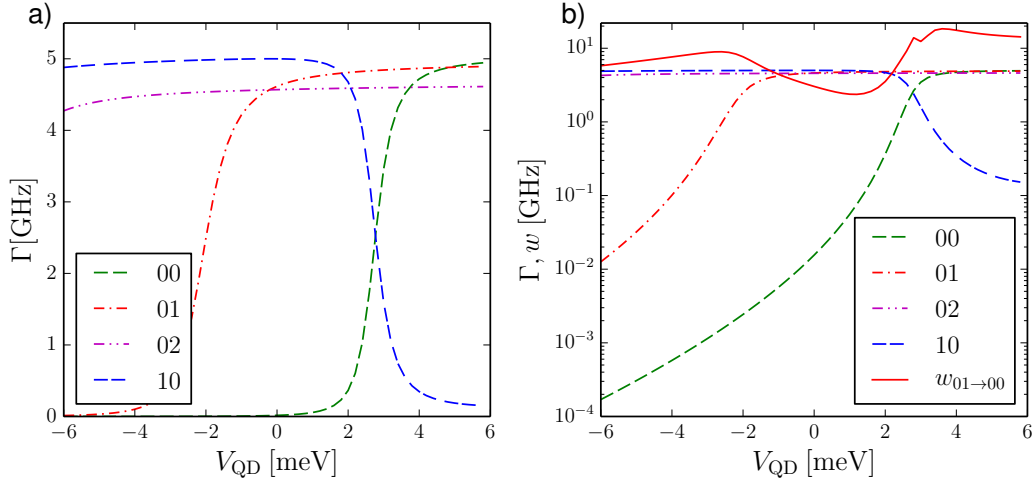


Figure 13. The couplings Γ between an electrode and particular states as functions of V_{QD} in linear (a) and logarithmic (b) scales. Additionally, the solid red line in the right panel represents the resulting relaxation rate.

Choosing $V_{QD} = -4$ meV (only two states in the bias window) for $\Gamma_E^D/\Gamma_E^S = 100$ we get from equations (24), (25) and (27) $I_F = 60$ fA, $I_R = 0.9$ fA, what gives $|I_F/I_R| = 64$.

In this reference situation we get very small currents because both the G and E states are placed in the inner part of the DRN (see figure 3a). To get a stronger current I_F we have to choose larger V_{QD} for which some excited states are placed in the outer part of the DRN resulting in the larger ratio of the respective tunneling rates $\Gamma_{E_i}^S/\Gamma_G^S$. For $V_{QD} > -2$ meV we have to consider three states in the bias window, as can be inferred from figure 2. Below we present two examples of our numerical results:

V_{QD}	Γ_E^D/Γ_E^S	I_F	I_R	$ I_F/I_R $	wave functions
1 meV	100	9 pA	0.09 pA	100	figure 3b
0 meV	200	4 pA	0.012 pA	320	

Table 1. Examples of model parameters and resulting currents.

The wave functions in these two cases differ only qualitatively and therefore only the case of $V_{QD} = 1$ meV is presented in figure 3b. The above example illustrates that it is possible to design a DRN that allows one to get a substantial forward current and a high degree of rectification. The Coulomb blockade due to the electron stuck in the

ground state will prevent from transport through any of the excited states in the reverse direction. On the other hand, they will all participate in the transport in the forward direction, what increases the total current. Because Γ_S^G is not exactly equal to zero, we get some leakage current in the reverse direction but still substantial rectifying behavior occurs.

The crucial requirement for the rectifier is the strong difference between the coupling to the ground state and to the excited states. This is the point where the advantage of the DRN over a QD is clearly visible. We performed, for comparison, calculations for QD with $R = 70$ nm, $\Gamma_E^D/\Gamma_E^S = 100$ and have got in the most favorable case: $I_F = 9$ pA, $I_R = 1.6$ pA, $|I_F/I_R| = 5.7$. One cannot obtain here a high degree of rectification because it is impossible to change the relative distribution of the ground and excited state wave functions in a QD. As a result, one cannot decrease the current I_R without simultaneous decreasing of I_F . In QDs the ratio Γ_E^S/Γ_G^S is usually below 10, whereas in the DRN the confining potential can be tuned to give Γ_E^S/Γ_G^S up to 10^3 . We see that the tunnel coupling to the reservoirs in the DRN is tunable over a much wider range than in QD. This, in turn, results in larger values of currents and more efficient rectification.

5. Summary

The fundamental requirement for future, low power consumption electronics is to control and manipulate single charges or spins. Quantum dots are the most popular and developed few-electron systems due to the relative easiness of fabrication and manipulation. On the other hand, the simple geometry of QDs allows modification of their electronic properties only to some extent, what encourages scientists to explore more complex systems like double or triple QDs. In this paper we performed systematic studies of electronic properties of a concentric dot-ring nanostructure and showed that, thanks to its non-trivial geometry, the structure offers unique possibilities to manipulate the electron wave functions. In particular, we have shown that by simple electrostatic gating one can move over the electron between the outer ring and the inner dot changing orbital relaxation by orders of magnitude and switching the character of a DRN from insulating to conducting. We have demonstrated that a DRN occupied by a single electron can be a good single electron transistor and a current rectifier with very high on/off ratio. The presented so called *wave function engineering* technique allows designing the properties of a system from the lowest quantum mechanical level. This is exactly how modern nanotechnology works and is the way to reach the limits of device miniaturization and to make the next step in development of quantum computers.

In the paper we present results for a DRN build as a InGaAs structure. However, the idea of a nanosystem where the wave functions can be moved over to different spatially separated parts can be applied also to other physical systems, for example graphene nanostructures [58–61]. We also neglect the spin effects. Yet, exploiting them would allow one to use a DRN in nanospintronics. The effect of spin on the Coulomb blockade has been studied in single QDs [5, 55, 62, 63] and in double QDs [29, 64, 65]. A

spin blockade in single electron transistor in QD resulting from spin polarized leads has been discussed in [66]. In the case of a DRN one would be able to independently control spin-up and spin-down quantum states, what would lead to spin dependent tunnel rates Γ . This, in turn, would give the possibility to control a spin polarised current.

By studying one-electron properties we have demonstrated that the structure offers the unique possibilities to manipulate the distribution of the wave functions what influences different DRN features. It also provides great flexibility in manipulating many-electron states, what, however, is out of the scope of this paper and will be presented elsewhere.

Acknowledgments

This work was supported by the National Science Centre (NCN) grant DEC-2013/11/B/ST3/00824. The authors thank K. Ensslin, T. Fujisawa, P. Hawrylak and J. Wróbel for fruitful discussions.

Appendix A. Derivation of the tunneling matrix element

According to Bardeen's approach [48] the tunneling matrix element is given by

$$t_{\mathbf{k}} = \frac{\hbar}{2m^*} \int_S d\vec{S} \cdot \left[\psi_{\mathbf{k}}^*(\mathbf{r}) \vec{\nabla} \Psi_{nl}(\mathbf{r}) - \Psi_{nl}(\mathbf{r}) \vec{\nabla} \psi_{\mathbf{k}}^*(\mathbf{r}) \right], \quad (\text{A.1})$$

what in two dimensions can be written as

$$t_{\mathbf{k}} = \frac{\hbar}{2m^*} \int_{-\infty}^{\infty} dy \left[\psi_{\mathbf{k}}^*(\mathbf{r}) \frac{\partial \Psi_{nl}(\mathbf{r})}{\partial x} - \Psi_{nl}(\mathbf{r}) \frac{\partial \psi_{\mathbf{k}}^*(\mathbf{r})}{\partial x} \right]_{x=x_0}, \quad (\text{A.2})$$

where $\Psi_{nl}(\mathbf{r})$ is the DRN's wave function and $\psi_{\mathbf{k}}(\mathbf{r})$ is the electrode's wave function. The electrodes are modelled as half-planes and their wave functions and eigenenergies are given by

$$\psi_{\mathbf{k}}(\mathbf{r}) = \frac{\sqrt{2}}{L} e^{ik_y y} \sin\left(\frac{\theta}{2}\right) e^{\kappa(x-x_1)}, \quad (\text{A.3})$$

$$\epsilon_{\mathbf{k}} = \frac{\hbar^2 k_y^2}{2m^*} + U - \frac{\hbar^2 \kappa^2}{2m^*}, \quad (\text{A.4})$$

where

$$\kappa = \frac{1}{\hbar} \sqrt{2m^* \left(U - \frac{\hbar^2 k_x^2}{2m^*} \right)}, \quad (\text{A.5})$$

$$\sin \theta = \frac{2\kappa k_x}{\kappa^2 + k_x^2}. \quad (\text{A.6})$$

The wave function of the DRN can be written as

$$\Psi_{nl} = R_{nl}(r) e^{il\phi} = R_{nl}(\sqrt{x^2 + y^2}) e^{il \arctan \frac{y}{x}}. \quad (\text{A.7})$$

The derivatives in equation (A.2) are given by

$$\frac{\partial \Psi_{nl}(\mathbf{r})}{\partial x} = \left[\frac{dR_{nl}(r)}{dr} \frac{x}{\sqrt{x^2 + y^2}} + R_{nl}(r) \frac{ily}{x^2 + y^2} \right] \exp \left(il \arctan \frac{y}{x} \right) \quad (\text{A.8})$$

and

$$\frac{\partial \psi_{\mathbf{k}}(\mathbf{r})}{\partial x} = \kappa \frac{\sqrt{2}}{L} e^{ik_y y} \sin \left(\frac{\theta}{2} \right) e^{\kappa(x-x_1)}. \quad (\text{A.9})$$

For each \mathbf{k} in equation (A.1) one has to calculate κ and θ [equations (A.5) and (A.6)], insert equations (A.3), (A.7), (A.8), and (A.9) into (A.2) and (numerically) calculate the integral. It is convenient to express $t_{\mathbf{k}}$ in polar coordinates where it takes the following form

$$t_{\mathbf{k}} = \frac{\sqrt{2}\hbar x_0}{2m^*L} \sin \left(\frac{\theta}{2} \right) e^{\kappa(x_0-x_1)} \int_{-\pi/2}^{\pi/2} d\phi \frac{e^{i(k_y x_0 \tan \phi + l\phi)}}{\cos^2 \phi} \times \left[R'_{nl} \left(\frac{x_0}{\cos \phi} \right) \cos \phi + R_{nl} \left(\frac{x_0}{\cos \phi} \right) \left(\frac{il \sin 2\phi}{2x_0} - \kappa \right) \right]. \quad (\text{A.10})$$

References

- [1] Kouwenhoven L, van der Vaart N, Johnson A, Kool W, Harmans C, Williamson J, Staring A and Foxon C 1991 *Z. Phys. B Condensed Matter* **85** 367
- [2] van der Vaart N C, Godijn S F, Nazarov Y V, Harmans C J P M, Mooij J E, Molenkamp L W, and Foxon C T 1995 *Phys. Rev. Lett.* **74** 4702
- [3] Devoret M H, Esteve D and Urbina C 1992 *Nature* **360** 547
- [4] Kastner M A 1992 *Rev. Mod. Phys.* **64** 849
- [5] Hanson R, Kouwenhoven L P, Petta J R, Tarucha S and Vandersypen L M K 2007 *Rev. Mod. Phys.* **79** 1217
- [6] Blais A, Huang R S, Wallraff A, Girvin S M and Schoelkopf R J 2004 *Phys. Rev. A* **69** 062320
- [7] Petta J R, Johnson A C, Taylor J M, Laird E A, Yacoby A, Lukin M D, Marcus C M, Hanson M P and Gossard A C 2005 *Science* **309** 2180
- [8] Versteegh M A M, Reimer M E, Jöns K D, Dalacu D, Poole P J, Gulinatti A, Giudice A and Zwiller V 2014 *Nature Communications* 5298
- [9] Schleser R, Ruh E, Ihn T, Ensslin K, Driscoll D C and Gossard A C 2005 *Phys. Rev. B* **72** 035312
- [10] Fujisawa T, Tokura Y and Hirayama Y 2001 *Physica B* **298** 573
- [11] Amasha S, MacLean K, Iuliana P, Zumbühl D M, Kastner M A, Hanson M P and Gossard A C 2008 *Phys. Rev. Lett.* **100** 046803
- [12] Fuhrer A, Lüscher S, Ihn T, Henzel T, Ensslin K, Wegscheider W and Bichler M 2001 *Nature* **413** 822
- [13] Scheibner R, Koenig M, Reuter D, Wieck A D, Gould C, Buhmann H and Molenkamp L W 2008 *New J. Phys.* **10** 083016
- [14] Lis K, Bednarek S, Szafran B and Adamowski J 2003 *Physica E* **17** 494
- [15] Averin D V and Likharev K K 1986 *Journal of Low Temperature Physics* **62** 345
- [16] Fulton T A and Dolan G J 1987 *Phys. Rev. Lett.* **59** 109
- [17] Fujisawa T, Austing D G, Tokura Y, Hirayama Y and Tarucha S 2002 *Nature* **419** 278
- [18] Koppens F H L, Buizert C, Tielrooij K J, Vink I T, Nowack K C, Meunier T, Kouwenhoven L P and Vandersypen L M K 2006 *Nature* **442** 766

- [19] Elzerman J M, Hanson R, van Beveren L H W, Witkamp B, Vandersypen L M K and Kouwenhoven L P 2004 *Nature* **430**
- [20] Weber C, Fuhrer A, Fasth C, Lindwall G, Samuelson L and Wacker A 2010 *Phys. Rev. Lett* **104** 036801
- [21] Shinkai G, Hayashi T, Hirayama Y and Fujisawa T 2007 *Appl. Phys. Lett* **90** 103116
- [22] McNeil R P G, Kataoka M, Ford C J B, Barnes C H W, Anderson D, Jones G A C, Farrer I and Ritchie D A 2011 *Nature Letters* **477** 103116
- [23] Hatano T, Stopa M, Yamaguchi T, Ota T, Yamada K and Tarucha S 2004 *Phys. Rev. Lett* **93** 439
- [24] Ota T, Ono K, Stopa M, Hatano T, Tarucha S, Song H Z, Nakata Y and Miyazawa T 2006 *Nature* **442** 766
- [25] Koppens F H L, Buizert C, Tielrooij K J, Vink I T, Nowack K C, Meunier T, Kouwenhoven L P and Vandersypen L M K 2004 *Phys. Rev. Lett* **93** 066801
- [26] Stopa M 2002 *Phys. Rev. Lett.* **88** 146802
- [27] Vidan A, Westervelt R M, Stopa M, Hanson M and Gossard A C 2004 *Appl. Phys. Lett* **85** 3602
- [28] Gaudreau L, Studenikin S A, Sachrajda A S, Zawadzki P, Kam A, Lapointe J, Korkusinski M and Hawrylak P 2006 *Phys. Rev. Lett* **97** 036807
- [29] Ono K, Austing D G, Tokura Y and Tarucha S 2002 *Science* **297** 1313
- [30] Johnson A C, Petta J R, Marcus C M, Hanson M P and Gossard A C 2005 *Phys. Rev. B* **72** 165308
- [31] Zipper E, Kurpas M, Sadowski J and Maška M M 2011 *J. Phys. Condens. Matter* **23** 115302
- [32] Kurpas M, Zipper E and Maška M M 2014 Engineering of electron states and spin relaxation in quantum rings and quantum dot-ring nanostructures *Physics of Quantum Rings* ed Fomin V M (Berlin, Heidelberg: Springer) p 455
- [33] Piacente G and Hai G Q 2007 *Phys. Rev. B* **75** 125324
- [34] Lei W, Notthoff C, Lorke A, Reuter D and Wieck A D 2010 *Appl. Phys. Lett* **96** 033111
- [35] Kleemans N A J M, Bominaar-Silkens I M A, Fomin V M, Gladilin V N, Granados D, Taboada A G, García J M, Offermans P, Zeitler U, Christianen P C M, Maan J C, Devreese J T and Koenraad P M 2009 *Phys. Rev. Lett* **99** 146808
- [36] Aharonov Y and Bohm D 1959 *Phys. Rev.* **115**
- [37] Büttiker M, Imry Y and Landauer R 1983 *Phys. Rev. A* **96** 365
- [38] Bluhm H, Koshnick N C, Bert J A, Huber M E and Moler K A 2009 *Phys. Rev. Lett.* **102** 136802
- [39] Birge N O 2009 *Science* **326** 244
- [40] Somaschini C, Bietti S, Koguchi N and Sanguinetti S 2011 *Nanotechnology* **22** 185602
- [41] Somaschini C, Bietti S, Koguchi N and Sanguinetti S 2010 *Appl. Phys. Lett.* **97** 203109
- [42] Lauhon L J, Gudiksen M S, Wang D and Lieber C 2002 *Nature* **420** 57
- [43] Dillen D C, Kim K, Liu E and Tutuc E 2014 *Nature Nanotechnology* **9** 116
- [44] Szafran B, Peeters F M and Bednarek S 2004 *Phys. Rev. B* **70** 125310
- [45] Zipper E, Kurpas M and Maška M M 2012 *New J. Phys.* **14** 093029
- [46] Kurpas M, Kędzierska B, Janus-Zygmunt I, Maška M M and Zipper E 2014 *Acta. Phys. Pol. A* **126** A-20
- [47] Janus-Zygmunt I, Kędzierska B, Gorczyca-Goraj A, Kurpas M, Maška M M and Zipper E 2014 *Acta. Phys. Pol. A* **126** 1171
- [48] Bardeen J 1961 *Phys. Rev. Lett.* **6** 57
- [49] Bockelmann U and Bastard G 1990 *Phys. Rev. B* **42** 8947
- [50] Stano P and Fabian J 2006 *Phys. Rev. B* **74** 045320
- [51] Hai G Q and Oliveira S S 2006 *Phys. Rev. B* **74** 193303
- [52] Hanson R, Vink I T, DiVincenzo D P, Vandersypen L M K, Elzerman J M, van Beveren L H W and Kouwenhoven L 2004 Determination of the tunnel rates through a few-electron quantum dot *Quantum Information and Decoherence in Nanosystems* ed Glattli D C, Sanquer M and Van J T T pp 145–150
- [53] Shavitt I 1977 *Methods of Electronic Structure Theory* (Plenum Press, New York) chap The Method

- of Configuration Interaction, pp 189 – 275
- [54] Fujisawa T, Tokura Y and Hirayama Y 2001 *Phys. Rev. B* **63** 081304(R)
 - [55] Weis J, Hang R H, v Klitzing K and Ploog K 1993 *Phys. Rev. Lett.* **71** 4019
 - [56] Yang C J and Gong W J 2013 *J. Korean Phys. Soc.* **63** 1175
 - [57] Mueller C R, Worschech L, Lang S, Stopa M and Forchel A 2009 *Phys. Rev. B* **80** 075317
 - [58] Molitor F, Güttinger J, Stampfer C, Dröscher S, Jacobsen A, Ihn T and Ensslin K 2011 *Journal of Physics: Condensed Matter* **23** 243201
 - [59] Stampfer C, Fringes S, Güttinger J, Molitor F, Volk C, Terrés B, Dauber J, Engels S, Schnez S, Jacobsen A, Dröscher S, Ihn T and Ensslin K 2011 *Frontiers of Physics* **6** 271–293 ISSN 2095-0462
 - [60] Trauzettel B, Bulaev D V, Loss D and Burkard G 2007 *Nat Phys* **3** 192–196 ISSN 1745-2473
 - [61] Ponomarenko L A, Schedin F, Katsnelson M I, Yang R, Hill E W, Novoselov K S and Geim A K 2008 *Science* **320** 356–358
 - [62] Johnson T, Kouwenhoven L P, de Jong W, de Vaart N C, Harmans C J P M and Foxon C T 1992 *Phys. Rev. Lett.* **69** 1592
 - [63] Weinmann D, Häsler W and Kramer B 1995 *Phys. Rev. Lett.* **74** 984
 - [64] Johnson A C, Petta J R, Markus C M, Hanson M P, and Gossard A C 2005 *Phys. Rev. B* **72** 165308
 - [65] Simmons C B, Koh T S, Shaji N, Thalakulam M, Klein L J, Qin H, Luo H, Savage D E, Lagally M G, Rimberg A J, Joynt R, Blick R, Friesen M, Coppersmith S N, and Eriksson M A 2010 *Phys. Rev. B* **82** 245312
 - [66] Ciorga M, Pioro-Ladriere M, Zawadzki P, Hawrylak P and Sachrajda A S 2002 *Appl. Phys. Lett.* **80** 2177